CDC01-REG1049

On Selecting Sensor and Actuator Locations for ANC in Ducts

V. Toochinda,* C.V. Hollot† and Y. Chait*

March 8, 2001

Abstract

In this paper we investigate the effects of microphone and speaker locations on the performance of active noise control in ducts. We study a so-called "symmetric" configuration in which the collocated performance microphone/control speaker and the collocated measurement microphone/disturbance source pairs are located equidistance from the duct center. By applying an "alignment angle" analysis to a duct model, we show this configuration to be prone to plant-disturbance misalignment. As a result, amplification at the measurement microphone and reduced stability margins occur. Stability robustness to modeling uncertainty is improved if the measurement microphone/disturbance source are de-collocated.

*MIE Department, University of Massachusetts, Amherst, MA 01003.
†ECE Department, University of Massachusetts, Amherst, MA 01003.

1 Introduction

Since the development of the digital computer, research in active noise control (ANC) has received much academic attention [1, 2]. In addition to its potential for commercial applications, knowledge gained from ANC system analysis can be applied to problems of similar nature; for example, control of flexible structures [3]. Of particular importance is the study of sensor and actuator configurations and their effect on closed-loop stability and performance. One such analysis was given in [4], where the relationship of microphone and speaker locations to closed-loop performance was discussed.

In this paper we examine the particular ANC configuration used in [5], which conforms with the preferred speaker/microphone location suggested in [4]. In a nutshell, the motivation for this configuration is that collocation of an actuator x and a sensor y renders the corresponding transfer function G_{yx} minimum phase and hence, free from the deleterious effect that right-half plane zeros have on closed-loop system properties [6]. Another suggestion from [4] is that collocation of actuators (or sensors) degrades closed-loop performance and hence undesirable. This motivated researchers to separate the actuators and sensors as far as possible. Taken together, these two constraints yield the symmetric speaker/microphone arrangement shown in Figure 1, which was used in [5]. The measurement microphone is collocated with the disturbance source, and the

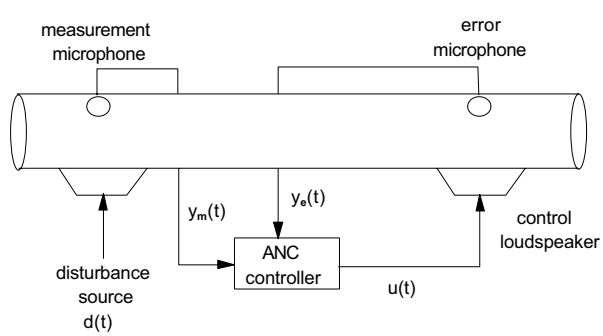

Figure 1: ANC system in a duct.

control speaker is collocated with the error microphone; then, these two speaker/microphone pairs are separated from each other. This configuration gives good closed-loop performance[1] at the error

[1]That is, the acoustic signal (due to disturbance d) at the error microphone is attenuated.

microphone. However, in [7] we have shown that significant amplification of the disturbance occurs at the measurement microphone, indicating poor stability robustness. This amplification occurs at frequencies where the plant[2] and disturbance are poorly aligned. In this paper we establish why this occurs and relate it to a particular configuration referred to as "misalignment-prone."

The paper is structured as follows. Section 2 briefly reviews a dynamic model for duct acoustics. This model will be the basis for our illustrative simulations. Sections 3 and 4 review our previous results relating plant-disturbance misalignment to closed-loop response, which is then used in Section 5 to study the symmetric configuration in Figure 1. In Section 6, we illustrate, by simulation example, that relaxing "symmetry" can improve stability robustness.

2 Model of duct acoustics

A basic configuration of an active noise control system consists of a duct with two loudspeakers and two microphones (see Figure 1). The upstream speaker simulates a disturbance source that injects acoustic "noise" into the duct. A measurement microphone detects the disturbance near the source while the downstream error microphone is located at a point where noise attenuation is desired. The ANC system uses the information provided by these two microphones to generate a signal sent to the control loudspeaker. The objective of the controller is to minimize the acoustic energy at the error microphone.

Consider the acoustic duct with dimensions as shown in Figure 2. Assume that the duct diameter is significantly smaller than its length. Then, as shown in [4], its dynamics can be described by a one-dimensional wave equation as

$$\frac{1}{c^2}p_{tt}(l,t) = p_{ll}(l,t) + \rho_0\dot{v}_u(t)\delta(l-L_u) + \rho_0\dot{v}_d(t)\delta(l-L_d)$$

where $p(l,t)$ is the acoustic pressure at location l meters from the upstream end of the duct, c is the phase speed of the acoustic wave ($343\,\frac{m}{s}$ in air at room conditions), $v_u(t)$ and $v_d(t)$ are the speaker cone velocities of the control speaker and the disturbance speaker, respectively, and ρ_0 is

[2] In our problem formulation the plant is defined as the dynamical system relating the control speaker input to the two microphone outputs. See Section 3 for more detail.

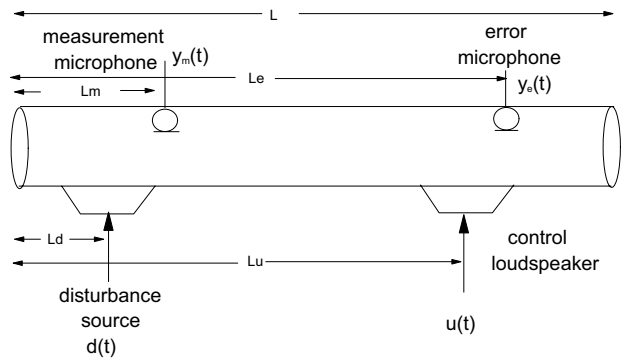

Figure 2: Acoustic duct.

the equilibrium density of air ($1.21\,\frac{kg}{m^3}$ at room conditions). Using separation of variables [8] and retaining r modal frequencies, $p(l,t)$ can be approximated by

$$p(l,t) \cong \sum_{i=0}^{r} q_i(t) V_i(l).$$

By introducing proportional damping, a state-space approximation is

$$\begin{aligned} \dot{x}(t) &= \mathbf{A}x(t) + \mathbf{B}u(t) + \mathbf{D}d(t) \\ y_e(t) &= \mathbf{E}x(t) \\ y_m(t) &= \mathbf{C}x(t) \end{aligned} \tag{1}$$

where

$$\begin{aligned} x(t) &= \begin{bmatrix} \int_0^t q_1(\sigma)d\sigma & q_1(t) & \ldots \int_0^t q_r(\sigma)d\sigma & q_r(t) \end{bmatrix}^T, \\ \mathbf{A} &= diag\left(\begin{bmatrix} 0 & 1 \\ -\omega_1^2 & 2\zeta_1\omega_1 \end{bmatrix}, ..., \begin{bmatrix} 0 & 1 \\ -\omega_r^2 & 2\zeta_r\omega_r \end{bmatrix} \right), \\ \mathbf{B} &= \frac{\rho_0}{A_s} \begin{bmatrix} 0 & V_1(L_u) & \ldots & 0 & V_r(L_u) \end{bmatrix}^T, \\ \mathbf{D} &= \frac{\rho_0}{A_s} \begin{bmatrix} 0 & V_1(L_d) & \ldots & 0 & V_r(L_d) \end{bmatrix}^T, \\ \mathbf{C} &= \begin{bmatrix} V_1(L_m) & 0 & \ldots & V_r(L_m) & 0 \end{bmatrix}, \\ \mathbf{E} &= \begin{bmatrix} V_1(L_e) & 0 & \ldots & V_r(L_e) & 0 \end{bmatrix} \end{aligned}$$

and

$$\omega_i = \frac{i\pi}{L}c, \quad V_i(l) = c\sqrt{\frac{2}{L}}\sin\frac{i\pi}{L}l, \quad i = 1, 2, 3, \ldots \quad .$$

A_s is the cross-sectional area of the speaker, L is the length of the duct and ζ_i is the proportional (viscous) damping of the ith acoustic mode.

To find a suitable model for controller design, we also require a transfer function model from the speaker voltage input V_s to the speaker baffle acceleration $\dot{v}_s$. This transfer function can be approximated, as in [8], by

$$P_s(s) = \frac{sv_s(s)}{V_s(s)} = \frac{K_s s^2}{s^2 + s\zeta_s\omega_s s + \omega_s^2}$$

where K_s is a speaker constant, ω_s is the natural frequency of the speaker and ζ_s is the damping ratio. By cascading this transfer function to the duct dynamics in (1) we have a working model of an ANC system. In the sequel we will use this model to simulate the closed-loop response to changes in actuator/sensor configurations. For simplicity, the dynamics of the microphones as well as the amplifier are assumed to be constant gains.

3 Performance analysis based on plant-disturbance misalignment

In this section we review our results from [7] where the properties of single-input two-output (SITO) feedback systems [9] were used to analyze the disturbance attenuation performance of an experimental ANC setup [5]. We start by formulating the duct (or plant) as a SITO system $\mathbf{P}(s)$ where the input is the control speaker input u and the outputs are the microphone signals y_m and y_e. Conversely, we view the controller as a two-input, single-output system $\mathbf{C}(s)$ with inputs y_m and y_e and output u. Their interconnection forms the feedback control system shown in Figure 3. The objective is to analyze the performance at y_m and y_e. We show that y_e is attenuated at the expense of amplification at y_m. Most importantly, this result holds independent of the controllers; it depends only on the configuration of microphones and control speakers.

To start, consider Figure 3 where $P_{ed}(s)$, $P_{eu}(s)$, $P_{md}(s)$, and $P_{mu}(s)$ are the transfer functions from the disturbance speaker to the error microphone, the control speaker to the error microphone, the disturbance speaker to the measurement microphone, and the control speaker to the measure-

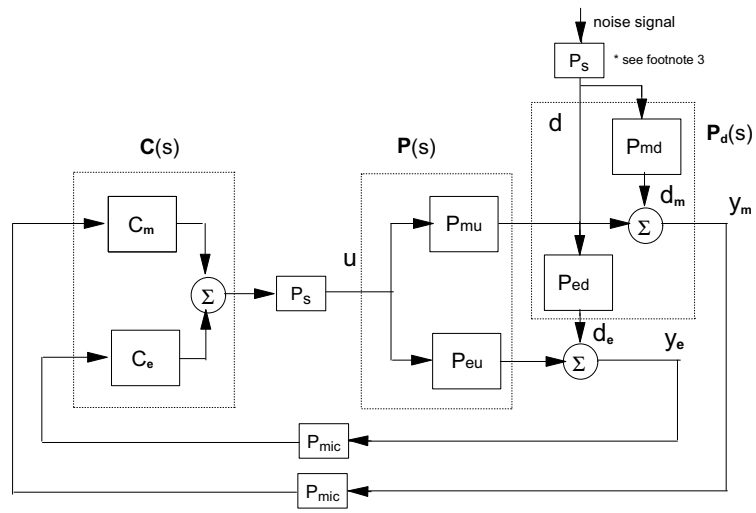

Figure 3: ANC as a single input, two output feedback system

ment microphone, respectively. P_{mic} and P_s represent microphone and speaker dynamics[3]. Let $C_m(s)$ denote the *feedforward* controller and $C_e(s)$ the *feedback* controller[4]. Further, define the plant, controller, and disturbance transfer functions as:

$$\mathbf{P}(s) \triangleq \begin{bmatrix} P_{mu}(s) \\ P_{eu}(s) \end{bmatrix}; \qquad \mathbf{C}(s) \triangleq [\ C_m(s) \quad C_e(s)\ ];$$

$$\mathbf{P}_d(s) \triangleq \begin{bmatrix} P_{md}(s) \\ P_{ed}(s) \end{bmatrix}.$$

Associated with this feedback system are several important transfer functions. These are the input and output loop transfer functions: $L_I(s) = \mathbf{C}(s)\mathbf{P}(s)$ and $\mathbf{L}_O(s) = \mathbf{P}(s)\mathbf{C}(s)$, the input and output sensitivity functions: $S_I(s) = (1 + L_I(s))^{-1}$ and $\mathbf{S}_O(s) = (\mathbf{I} + \mathbf{L}_O(s))^{-1}$, and the input and output complementary sensitivity functions: $T_I(s) = L_I(s)(1+L_I(s))^{-1}$ and $\mathbf{T}_O(s) = \mathbf{L}_O(s)(I+\mathbf{L}_O(s))^{-1}$. The transfer functions at the plant input are scalar, while those at the plant output are 2 x 2.

We define the attenuation factor as the ratio of closed-loop to open-loop response

$$\alpha(\omega) \triangleq \frac{||\mathbf{S}_O(j\omega)\mathbf{P}_d(j\omega)||}{||\mathbf{P}_d(j\omega)||}. \tag{2}$$

[3]Though in real ANC applications we do not have the speaker transfer function at the disturbance source, our alignment angle analysis still holds.

[4]In the ANC literature, the action taken on the measurement microphone signal y_m is referred to as "feedforward" control, while action taken on y_e is called "feedback" control. See [7] for more explanation on this terminology.

The attenuation factor is used as a measure of closed-loop performance; i.e., $\alpha(\omega) < 1$ implies attenuation while $\alpha(\omega) > 1$ indicates amplification of the disturbance. We also need the notion of alignment angles from [9].

Definition 1: The *plant-controller alignment* angle (at frequency ω) is

$$\phi_{pc}(j\omega) \triangleq \cos^{-1}\left(\frac{|\mathbf{C}(j\omega)\mathbf{P}(j\omega)|}{||\mathbf{C}(j\omega||||\mathbf{P}(j\omega)||}\right) \tag{3}$$

while the *plant-disturbance alignment* angle is

$$\phi_{pd}(j\omega) \triangleq \cos^{-1}\left(\frac{|\mathbf{P}^H(j\omega)\mathbf{P}_d(j\omega)|}{||\mathbf{P}(j\omega||||\mathbf{P}_d(j\omega)||}\right). \tag{4}$$

The plant and controller (plant and disturbance) are said to be *perfectly aligned* if $\phi_{pc}(j\omega) = 0^\circ$ ($\phi_{pd}(j\omega) = 0^\circ$), and *completely misaligned* if $\phi_{pc}(j\omega) = 90^\circ$ ($\phi_{pd}(j\omega) = 90^\circ$). We now state the main result from [7].

Proposition 1: *If* $|y_e(j\omega)| = 0$ *and* $\phi_{pd}(j\omega) = 90^\circ$, *then*

$$\frac{|y_m(j\omega)|}{||\mathbf{P}_d(j\omega)||} = \alpha(\omega) \geq \sqrt{1 + \left|\frac{P_{ed}(j\omega)}{P_{md}(j\omega)}\right|^2}. \tag{5}$$

From Proposition 1 we see that under perfect cancelation, $y_m(j\omega)$ is amplified if the plant and disturbance transfer functions are completely misaligned. Furthermore, if $|P_{ed}(j\omega)| \gg |P_{md}(j\omega)|$, then $|y_m(j\omega)|$ is large.

4 Stability margins

In the last section we concentrated on performance analysis and presented a situation where $|y_m(j\omega)|$ becomes large as $|y_e(j\omega)|$ approaches zero. Specifically, we saw that $|y_m(j\omega)|$ peaks at the frequency where $\phi_{pd}(j\omega) \approx 90^\circ$ and the ratio $\frac{|P_{ed}(j\omega)|}{|P_{md}(j\omega)|}$ has a maximum. As a result, we would expect smaller stability margins (or larger $||\mathbf{S}_O(j\omega)||_\infty$) at this frequency. Therefore, our stability analysis is focused on the condition $\phi_{pd}(j\omega) \approx 90^\circ$ and $\frac{|P_{ed}(j\omega)|}{|P_{md}(j\omega)|} \gg 1$. In this section we study the output sensitivity $\mathbf{S}_O(j\omega)$ whose size $||\mathbf{S}_O(j\omega)||_\infty$ provides one measure of stability margin;

e.g., see [11]. Of equal importance is the size of output complementary sensitivity $||\mathbf{T}_O(j\omega)||_\infty$. Note that $||.||_\infty$ is bounded below by the magnitude response of each element of the corresponding transfer function. In our case, $||\mathbf{S}_O(j\omega)||_\infty$ ($||\mathbf{T}_O(j\omega)||_\infty$) becomes large as a result of the element S_{O11} (T_{O11}). Having $||T_{O11}||_\infty$ large, for example, indicates poor robustness to multiplicative plant uncertainty in P_{mu}.

We separate the analysis into two cases: feedforward, and feedforward/feedback control.

Case 1: (feedforward; $\mathbf{C}(j\omega) = [C_m(j\omega) \;\; 0]$) In this case, the system's closed-loop response is given by

$$\mathbf{S}_O(j\omega) = \begin{bmatrix} S_I(j\omega) & 0 \\ -\frac{P_{eu}(j\omega)}{P_{mu}(j\omega)} T_I(j\omega) & 1 \end{bmatrix}. \tag{6}$$

Now, suppose $|y_e(j\omega)| = 0$. Then, as shown in [7]:

$$|T_I(j\omega)| = \frac{|P_{ed}(j\omega)P_{mu}(j\omega)|}{|P_{md}(j\omega)P_{eu}(j\omega)|} \approx \left|\frac{P_{ed}(j\omega)}{P_{md}(j\omega)}\right|^2. \tag{7}$$

With $\frac{|P_{ed}(j\omega)|}{|P_{md}(j\omega)|} \gg 1$, it follows from the fundamental algebraic constraint $S_I(j\omega) + T_I(j\omega) = 1$ that $|S_I(j\omega)| \gg 1$. This in turn implies that $||\mathbf{S}_O(j\omega)|| \gg 1$. Thus, whenever we use feedforward control, $\mathbf{C}(j\omega) = [C_m(j\omega) \;\; 0]$, attenuation of $|y_e(j\omega)|$ at a frequency where both $\frac{|P_{ed}(j\omega)|}{|P_{md}(j\omega)|} \gg 1$ and plant-disturbance are misaligned necessarily leads to reduced stability margins.

Case 2: (feedforward and feedback control; $\mathbf{C}(j\omega) = [C_m(j\omega) \;\; C_e(j\omega)]$) Using straightforward manipulations, the output sensitivity and complementary sensitivity functions can be written as

$$\mathbf{S}_O(s) = \mathbf{I} - S_I(s)\mathbf{L}_O(s)$$

and

$$\mathbf{T}_O(s) = S_I(s)\mathbf{L}_O(s)$$

where

$$\mathbf{S}_O(j\omega) = \begin{bmatrix} S_{O11}(j\omega) & -\frac{P_{mu}(j\omega)}{P_{eu}(j\omega)} T_{O22}(j\omega) \\ -\frac{P_{eu}(j\omega)}{P_{mu}(j\omega)} T_{O11}(j\omega) & S_{O22}(j\omega) \end{bmatrix} \tag{8}$$

and where $S_{Oij}(j\omega)$ and $T_{Oij}(j\omega)$ are the (i,j)th element of $\mathbf{S}_O(j\omega)$ and $\mathbf{T}_O(j\omega)$, respectively. Note the similarities and differences to (6); e.g., S_{O11} and T_{O11} in (8) plays the same role as S_I and T_I in (6) because of the algebraic constraint. We state without proof the following result from [7].

Proposition 2: *If* $|y_e(j\omega)| = 0$*, then*

$$|T_{O11}(j\omega)| = \frac{|\frac{P_{mu}(j\omega)}{P_{eu}(j\omega)}|}{\left|\frac{P_{md}(j\omega)}{P_{ed}(j\omega)} + \frac{C_e(j\omega)}{C_m(j\omega)}\right|}. \tag{9}$$

Proposition 2 shows that for perfect attenuation, $|T_{O11}(j\omega)|$ depends not only on plant and disturbance transfer functions but also on both controllers. Therefore, unlike Case 1, the ratio $\frac{|P_{mu}(j\omega)|}{|P_{eu}(j\omega)|}$ does not impose a constraint on $|T_{O11}(j\omega)|$.

Remark 1: It is interesting to note that in the feedforward case, stability margins depend only on the magnitude ratio of P_{ed} and P_{md} and not on the controller; see (7). In contrast, Proposition 2 shows that the use of both feedforward and feedback affect stability margins. In experiments we have shown [7] that using both feedforward and feedback controllers significantly improves stability margins. Having noted this, we also realize that feedforward control schemes are prevalent in ANC practice, and in the last section of this paper we demonstrate how their stability margins are improved by modifying microphone-speaker configurations.

5 Misalignment-prone configuration

Equipped with the theoretical preliminaries from the previous sections, we are now ready to tackle the closed-loop system properties in terms of microphone-speaker configurations. Consider the situation below where two collocated pairs of microphone-speakers are symmetrically configured about the duct center. We assign numerical values to variables to the duct model as in Figure 4; i.e., let $L = 0.85$ meters, $L_d = L_m = 0.15$ meters, and $L_e = L_u = 0.70$ meters. The speaker parameters

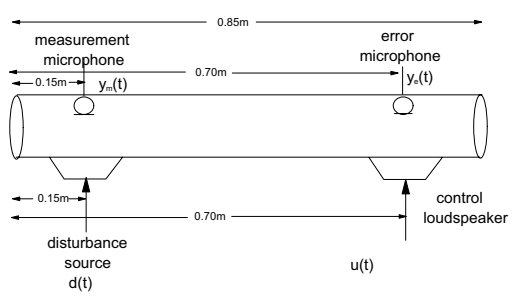

Figure 4: Acoustic duct configuration with symmetric collocated microphone/speaker pairs.

are chosen as in [8] with modal frequency = 67 Hz and damping ratio 0.74. Microphone dynamics are ignored. Substituting these values into the duct model in Section 2, we obtain the four transfer functions $P_{ed}(s)$, $P_{eu}(s)$, $P_{md}(s)$, and $P_{mu}(s)$. The controllers C_m and C_e are designed using the H_∞ synthesis technique [10]. The closed-loop frequency response at output y_m and y_e are shown in Figure 5 which are similar to those in [7]; that is, attenuation at the performance output y_e

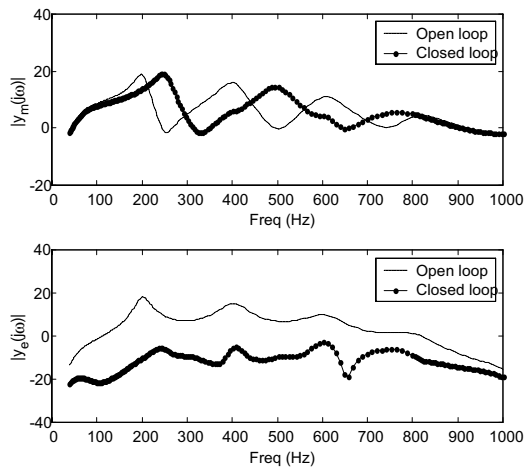

Figure 5: Comparison of $y_m(j\omega)$ and $y_e(j\omega)$ for symmetric duct configuration.

is achieved at the expense of amplification in y_m. As discussed above, this peaking is related to $||S_O||_\infty$, a measure of stability margin. Figure 6 shows the plant-disturbance alignment angle and the disturbance gain ratio $\frac{|P_{ed}|}{|P_{md}|}$. Recall from Proposition 1 that amplification in y_m occurs at a frequency where the plant and disturbance are misaligned and $|P_{ed}| >> |P_{md}|$. Figure 5 and 6 shows the existence of this critical frequency at 250 Hz. In this regard, we can use the plant-disturbance misalignment angle ϕ_{pd} and the disturbance gain ratio as a measure of closed-loop performance. As ϕ_{pd} approaches 90°, y_m is subject to amplification; the degree of amplification is related to the disturbance gain ratio. The following proposition explains why the symmetric configuration is susceptible to plant-disturbance misalignment.

Proposition 3: *Consider a duct configuration as in Figure 4 where microphone/speaker pairs are collocated and symmetric about the duct center; i.e., $L_d = L_m = x$ and $L_u = L_e = L - x$. Then, the plant and disturbance are completely misaligned when the phase difference between $P_{ed}(s)$ and $P_{eu}(s)$ (or between $P_{ed}(s)$ and $P_{md}(s)$) equals $\pm(\frac{1}{2} + 2n)\pi$, $n = 0, 1, 2, \ldots$.*

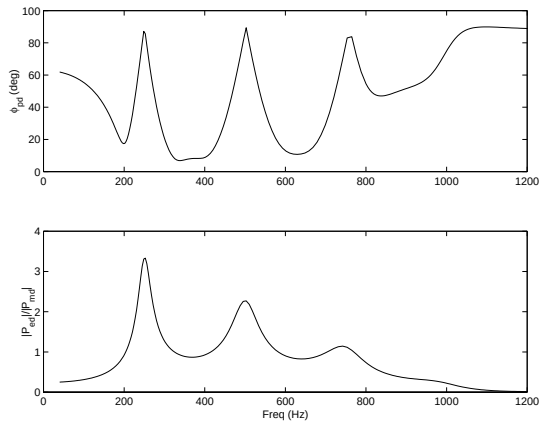

Figure 6: Plant-disturbance alignment angle and $\frac{|P_{ed}|}{|P_{md}|}$ plots.

Proof: From (4), $\phi_{pd}(j\omega) = 90^\circ$ when $\bar{P}_{mu}(j\omega)P_{md}(j\omega) + \bar{P}_{eu}(j\omega)P_{ed}(j\omega) = 0$.[5] It is straightforward to verify that $P_{ed} = P_{mu} \triangleq a\angle\psi$ and $P_{eu} = P_{md} \triangleq b\angle\theta$. Hence $\bar{P}_{mu}P_{md} + \bar{P}_{eu}P_{ed} = ab\angle{-(\psi-\theta)} + ab\angle(\psi-\theta) = 0$ when $\psi - \theta = \pm(\frac{1}{2} + 2n)\pi,\ \ n = 0, 1, 2, \ldots$. □

Proposition 3 states that symmetric duct configurations are inherently misalignment-prone since the condition $\phi_{pd}(j\omega) = 90^\circ$ is determined solely by the phases of plant and disturbance transfer functions. In Figure 7 we plot the magnitude and phase of P_{ed} and P_{md} (see Remark 2 below). The comparison suggests that misalignment is likely to occur in symmetric configurations since P_{ed} and P_{md} share the same poles while the former is nonminimum phase and the latter minimum phase. As seen from Figure 7, the phases of these transfer functions are similar in low frequency region. After the first modal frequency, a RHP zero in P_{ed} results in additional phase lag. At 250 Hz, this difference equals 90° and the first instance of complete misalignment occurs. As the phase lag of P_{ed} increases with frequency, misalignments occur again at 500 Hz and 750 Hz.

Remark 2: The reason we choose to compare P_{ed} and P_{md}, instead of P_{ed} and P_{eu} in Figure 7,[6] is that the disturbance gain ratio $\frac{|P_{ed}|}{|P_{md}|}$ can be readily observed in the same plot. Interestingly, Figure 7 indicates that $|P_{ed}| >> |P_{md}|$ at those frequency points where misalignment occurs. The peaks in $\frac{|P_{ed}|}{|P_{md}|}$ coincide with the peaks of ϕ_{pd}; see Figure 6. This is unfavorable in view of constraints (5) and (7).

[5] Overbar denotes complex conjugate.

[6] Recall that $P_{md} = P_{eu}$ in the symmetric configuration.

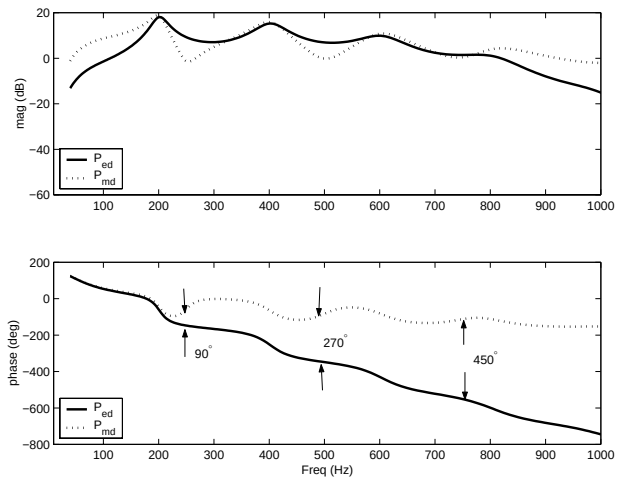

Figure 7: Magnitude and phase comparison of P_{ed} and P_{md}.

The symmetry assumption in Proposition 3 may appear artificial, especially from an ANC application viewpoint. However, the preference for collocation and separation as suggested in [4] tends to force this structure. For instance, even if it were not feasible to collocate the y_m microphone with the disturbance, one may be tempted to install the microphone as close to the disturbance source as possible. The result is a duct configuration which is only slightly perturbed from symmetry. We have determined via computer simulation that plant-disturbance misalignment persists even when the position of collocated microphone/speaker pairs is shifted. To demonstrate, we create some MATLAB code to compute the alignment angle as a function of the location of collocated error microphone/control speaker pair in the range of 0.4 to 0.8 meters. The collocated measurement microphone/disturbance source pair was fixed at $L_d = L_m = 0.15$ meters. We observed that P_{mu} always equal P_{ed}, but P_{md} and P_{eu} differ once symmetry is violated. Figure 8 shows the plot of $\max_\omega \phi_{pd}$ and the disturbance gain ratio $\frac{|P_{ed}|}{|P_{md}|}$ versus the $L_e = L_u$ locations. We see that $\max_\omega \phi_{pd}$ remains close to 90° in a fairly broad vicinity of the symmetric point $L_e = L_u = 0.70$ meters. The disturbance gain ratio is also significant in this region.

We conclude from this observation that a configuration with both microphone/speaker pairs collocated may not be preferred insofar as stability robustness is concerned. Therefore, we seek an alternative configuration with improved stability margins while maintaining comparable performance. An immediate suggestion is to de-collocate one of the two pairs. We want to keep error

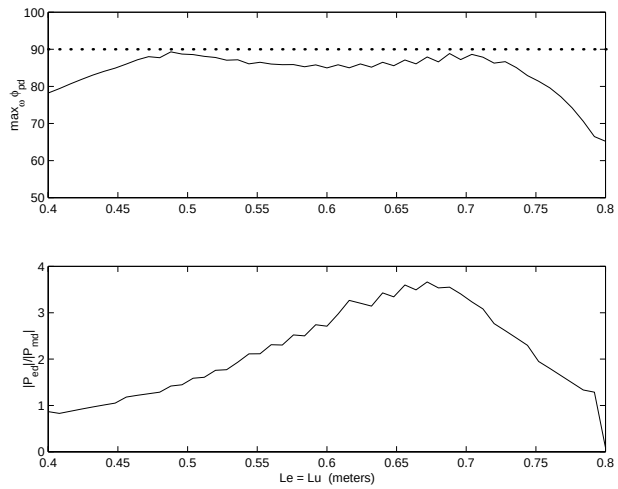

Figure 8: $\max_\omega \phi_{pd}$ and $\frac{|P_{ed}|}{|P_{md}|}$ versus $L_e = L_u$ locations for "symmetric" duct configuration.

microphone and control speaker collocated because this renders P_{eu} minimum phase and allows attenuation to be achieved at y_e, our primary performance objective. As a result, we propose in the next section a new configuration where the collocation between the disturbance source and measurement microphone is relaxed. Simulation results show stability margins are improved from the symmetric case.

6 Simulation example: feedforward controller

The acoustic duct model developed in Section 2 is used to simulate the effect of microphone/speaker locations to closed-loop properties. Here we focus only on the SISO controller structure $\mathbf{C}(j\omega) = [C_m(j\omega) \quad 0]$ for the following reasons. Firstly, feedforward control is the most common scheme for ANC. Secondly, stability margins for this SISO controller do not depend on the controller; see Remark 1. Thus, it is more illuminating to compare the effect of microphone/speaker locations to closed-loop stability and performance. Moreover, analysis in [7] reveals that this SISO controller has larger $||S_O||_\infty$ and $||T_O||_\infty$ and hence poorer stability robustness than the TISO controller case.

Using the same set of weighting functions, we perform H_∞ design for both the symmetric duct in Figure 4 and the new proposed configuration shown in Figure 9 where we un-collocate the disturbance source and measurement microphone. The speaker transfer functions are chosen

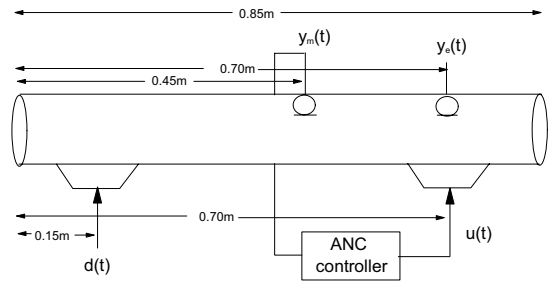

Figure 9: Acoustic duct configuration with noncollocated disturbance/measurement microphone.

with the same parameters as in the previous section and the microphone and amplifier dynamics are ignored. We choose $L_m = 0.45$ m ; i.e., y_m is moved towards y_e, but not collocated, since [4] suggests that collocation of y_m and y_e results in closed-loop amplification. Figure 10 compares the closed-loop performance y_e of these two configurations. On the average they are quite comparable,

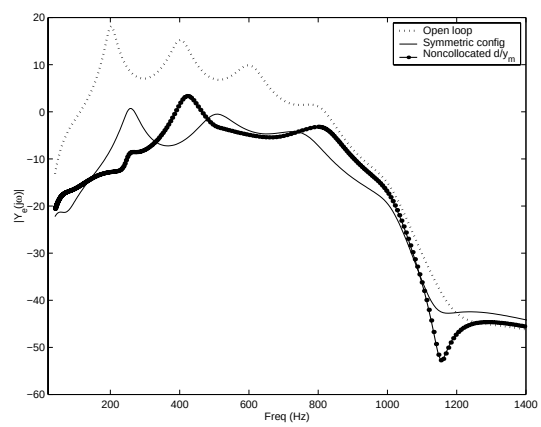

Figure 10: Comparison of closed-loop performance at y_e.

especially in the low frequency region. However, lets do more analysis. As seen from Figure 11, the maximum plant-disturbance alignment angle ϕ_{pd} for the new duct configuration decreases slightly from the symmetric case, but the peaking in ϕ_{pd} and $\frac{|P_{ed}|}{|P_{md}|}$ no longer occur at the same frequency. This is a good omen for improved stability margins[7], which can be measured by the size of $||S||_\infty$ and $||T||_\infty$.[8] Large $||T||_\infty$, for instance, results in poor robustness to multiplicative plant uncertainty in P_{mu}. Figure 12 compares the magnitude frequency response $|S(j\omega)|$ and $|T(j\omega)|$ between the two

[7]See (5) in Proposition 1.

[8]Since this simulation example is a SISO feedback system, we can restrict our attention to $S_I(s)$ and $T_I(s)$; see (6) and (7).

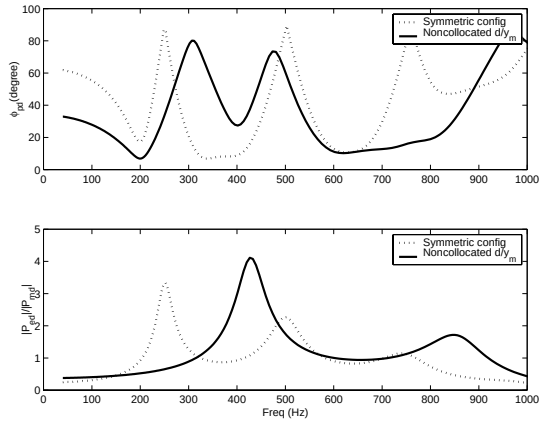

Figure 11: Comparison of plant-disturbance alignment angle and disturbance gain ratio.

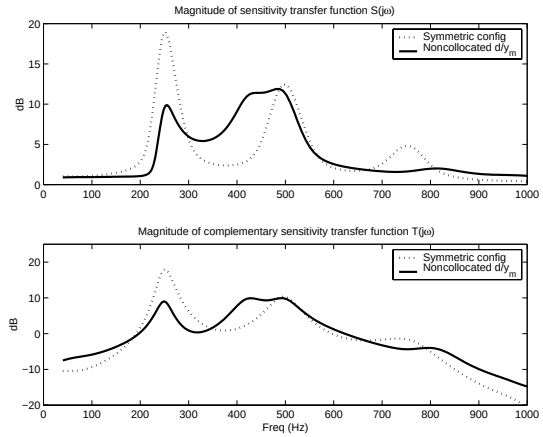

Figure 12: Frequency responses of the sensitivity and complementary sensitivity functions.

configurations. We see that when y_m and d are not collocated, $||S||_\infty$ is reduced from 16 dB to 12 dB and $||T||_\infty$ from 18 dB to 10 dB. In classical stability analysis, $||S||_\infty$ is interpreted as the inverse of the distance of the loop frequency response to the critical point. Hence, large $||S||_\infty$ indicates poor stability margin. A comparison of Nyquist plots is shown in Figure 13. By using the same scale we can see that the frequency response of the loop transfer function $L(s) = C_m(s)P_{mu}(s)$ for the symmetric configuration case is closer to the critical point $-1 + j0$ than that of the noncollocated case. In the symmetric case, the gain margin is 1.08 dB and the phase margin is 15.7 degree, while in the noncollocated d/y_m case, the gain margin is improved to 3.21 dB and the phase margin is 21.2 degree.

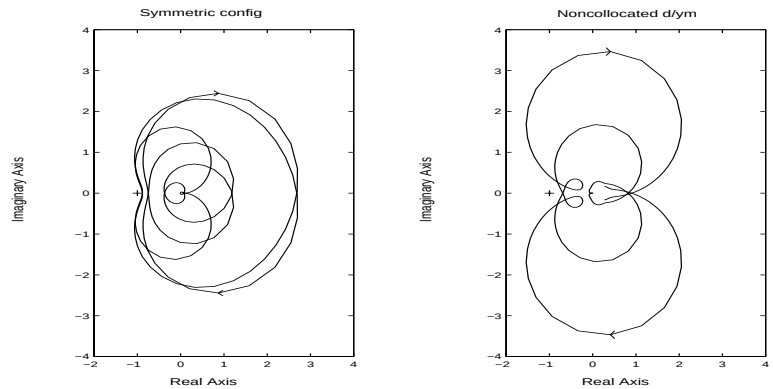

Figure 13: Comparison of Nyquist plots.

7 Conclusions

This paper suggests an application of results in [7] to the selection of a configuration for ANC in ducts that yields good overall performance plus improved stability margins. The plant-disturbance alignment does not depend on controllers, and allows us to evaluate fundamental limitations of ANC before the control design phase. This is useful because installing sensors and actuators can be a time-consuming and costly process, involving precision machining which permanently altering the duct dynamics. Often a control engineer realizes too late that the chosen configuration imposes inherent performance limitations and a time were options are made few.

Though the result in Proposition 3 holds only in the case of symmetric configurations, our plant-disturbance alignment approach applies to arbitrary configurations; i.e., one simply evaluates $\phi_{pd}(j\omega)$ over the possible arrangements. A rule of thumb is to avoid those configurations where misalignment and peaking in the disturbance gain ratio $\frac{|P_{ed}|}{|P_{md}|}$ occur at the same frequency.

Applying the analysis of SITO systems to active noise control is still a novel approach. There is more work to be done. We hope that our present work paves a way for future research towards an efficient integrated ANC system design.

References

[1] S.M. Kuo and D. R. Morgan, *Active Noise Control Systems*, Wiley-Interscience, New York, 1996.

[2] P.A. Nelson and S. J. Elliott, *Active Control of Sound*, Academic Press, London, 1992.

[3] S.O.R. Moheimani, H.R. Pota, and I. R. Petersen, "Active Control of Noise and Vibration in Acoustic Ducts and Flexible Structures - A Spatial Control Approach," *American Control Conference*, pp. 2601 - 2605, 1998.

[4] J. Hong and D.S. Bernstein, "Bode Integral Constraints, Colocation, and Spillover in Active Noise and Vibration Control," *IEEE Trans. Control Systems Technology*, Vol. 6 (1), pp. 111-120, 1998.

[5] T. Klawitter, *Linear Active Duct Noise Control: Feedforward/Feedback Controllers Designed with H_∞ and Quantitative Feedback Theory,* M.S. Thesis, University of Massachusetts, Amherst, 2000.

[6] J.S. Freudenberg and D.P. Looze, "Right Half Plane Poles and Zeros and Design Tradeoffs in Feedback Systems,"*IEEE Trans. Automatic Control*, Vol. AC-30(6), pp. 555-565, 1985.

[7] V. Toochinda, T. Klawitter, C.V. Hollot and Y.Chait, "A Single-Input Two-Output Feedback Formulation for ANC Problems," to appear in *Proceedings of the American Control Conference*, Arlington, VA, 2001.

[8] J. Hong, J.C. Akers, R. Venugopal, M. N. Lee, A. G. Sparks, P.D. Washabaugh, and D.S. Bernstein, "Modeling, Identification, and Feedback Control of Noise in an Acoustic Duct," *IEEE Trans. Contr. Sys. Tech.*, Vol. 4, pp. 283 -291, 1996.

[9] J.S. Freudenberg and R.H. Middleton, "Properties of Single Input, Two Output Feedback Systems," *International Journal of Control*, Vol. 72 (16) pp. 1446-1465, 1999.

[10] R.Y. Chiang and M.G. Safonov, *Robust Control Toolbox*, The MathWorks, Natick, MA, 1992.

[11] J.C. Doyle, B.A. Francis and A.R. Tannenbaum, *Feedback Control Theory,* Macmillan, New York, 1992.